Joint reconstruction with a correlative regularisation technique for multi-channel neutron tomography

Evelina Ametova[1,2,*], Genoveva Burca[3,4], Gemma Fardell[5], Jakob S. Jørgensen[4,6], Evangelos Papoutsellis[1,5], Edoardo Pasca[5], Ryan Warr[1], Martin Turner[7], William R. B. Lionheart[4], and Philip J. Withers[1]

[1]Henry Royce Institute, Department of Materials, The University of Manchester, United Kingdom
[2]Laboratory for Application of Synchrotron Radiation, Karlsruhe Institute of Technology, Germany
[3]ISIS Pulsed Neutron and Muon Source, STFC, UKRI, Rutherford Appleton Laboratory, United Kingdom
[4]Department of Mathematics, The University of Manchester, Manchester, United Kingdom
[5]Scientific Computing Department, STFC, UKRI, Rutherford Appleton Laboratory, United Kingdom
[6]Department of Applied Mathematics and Computer Science, Technical University of Denmark, Denmark
[7]Research IT Services, The University of Manchester, United Kingdom

Abstract Time-of-flight (ToF) energy-dispersive neutron tomography is complimentary to X-ray tomographic imaging method aimed at the reconstruction of wavelength-dependent material response in every three-dimensional volume element. ToF neutron tomography has already demonstrated great potential for both mapping of crystallographic properties and elemental composition in micrometer scale. However, available neutron beams have inherently low fluxes and high ToF resolution comes at the cost of prohibitively long exposure times. In this paper we investigate application of advanced iterative reconstruction algorithms with both spatial and spectral regularisation to reduce exposure time. The capability of advanced reconstruction algorithms is demonstrated on a specifically designed multi-material sample.

2 Introduction

Time-of-flight (ToF) energy-dispersive neutron computed tomography (CT) provides a complimentary technique to X-ray CT. As neutrons interact with atomic nuclei rather than an atom's electron cloud and can penetrate materials at wavelengths comparable to lattice spacings, they can be used to investigate the chrystallographic structure of materials. Governed by Bragg's law, coherent elastic scattering produces characteristic jumps in the transmitted neutron spectrum at wavelength equal twice the spacing between lattice planes. As neutrons are uncharged particles and can penetrate much deeper into material than X-rays, they allow to probe atomic structures in bulk samples. In fig. 1, left, we show the wavelength-dependent macroscopic total neutron cross-section $\Sigma_{\text{tot}}(\lambda), [\text{cm}^{-1}]$ for materials employed in the present study. The neutron cross-section defines probability of interactions to occur, *i.e.* decrease in transmitted intensity. Such acquisition is also commonly called Bragg-edge neutron CT due to characteristic shape of the transmitted spectrum.

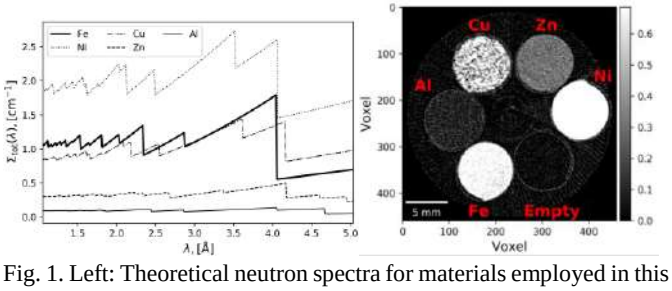

Fig. 1. Left: Theoretical neutron spectra for materials employed in this study. Right: White beam (sum of all channels) reconstruction of the sample cross-section with the conventional FBP method. Colour range was adjusted to highlight low intensity features.

ToF imaging utilises a pulsed neutron source and measures arrival time of each neutron with respect to the pulse. Pixellated counting ToF detector discretises recorded information into pixel elements, each counting the individual incident neutrons and registers each of them in one of multiple ToF channels depending on arrival time. ToF values are subsequently converted into wavelength values. Data acquisition in ToF neutron CT is very time consuming since neutron fluxes are typically low (compared to synchrotron X-ray sources) and because the detected neutrons are shared among multiple ToF channels. Thus, prohibitively long exposure time (in order of several hours per projection) is needed to acquire sufficiently high counts in each ToF channel. In practice, shorter exposure is used and acquired multi-channel projections are binned, in spatial and/ or spectral dimension, to improve signal-to-noise ratio [1, 2].

Regularised iterative reconstruction has already proven to be a viable approach to improve reconstruction quality from noisy and/or undersampled data in X-ray CT. Iterative reconstruction formulates reconstruction as an optimisation problem and allows to incorporate available prior knowledge to produce satisfactry results for otherwise unsolvable tomographic problems. In spectral tomography, priors exploiting structural similarities across energy channels are particularly promising. Here, we investigate application of two regularisation techniques: Total Nuclear Variation (TNV) and a dedicated tailored regularisation technique. The former method is a recent regulariser for reconstructing spectral CT images which enforces common edges across all channels [3-5]. The second technique is specifically tailored for Bragg edge neutron CT and combines Total Variation (TV) regularisation [6, 7] in the spatial dimension and Total Generalised Variation (TGV) regularisation [8] in the spectral dimension. TV preserves edges and suppresses noise by encouraging sparsity in the finite difference domain, while TGV regularisation promotes characteristic piece-wise smooth behaviour in the spectral dimension. Implementation of the advanced reconstruction methods has been made possible by the CCPi Core Imaging Library (CIL) reconstruction framework [9, 10]. The capability of advanced

reconstruction algorithms is demonstrated on a specifically designed multi-material sample consisting of aluminium cylinders filled with metallic powder of high purity (fig. 1, right). Although the case study has been performed on a single two-dimensional slice, the results can be generalised to the third dimension.

2 Materials and methods

2.1. Data acquisiton

The dataset in the present study was imaged at the Imaging and Materials Science & Engineering (IMAT) beamline operating at the ISIS spallation neutron source (Rutherford Appleton Laboratory, U.K.) [11, 12]. The ToF detector [13] has 512×512 active pixels, 0.055 mm pixel size. The detector was configured to measure 2843 energy channels between 1 Å and 5 Å with wavelength resolutions between $0.7184{\cdot}10^{-3}$ Å and $2.8737{\cdot}10^{-3}$ Å. A set of spectral projections was acquired at 120 equally-spaced angular positions over 180° rotation. Each projection was acquired with 15 min exposure time. Additionally, 8 flat field images (4 before and 4 after the sample acquisition) were recorded with the same settings. Detector related corrections [14] and flat field correction were applied to all projections. Finally, spectral images were cropped spatially to 460 pixels and binned in the spectral dimension to 339 channels with a uniform bin width of $11.5{\cdot}10^{-3}$ Å.

In fig. 2 (upper row) we demonstrate sinograms for selected individual wavelength channels. Spanning the most valuable spectral range for the present sample, they show differences in noise levels and intensity of features depending on wavelength. The incident spectrum on IMAT has a crude "bell shape" with a peak around 2.6 Å [11, 12]. Therefore the elevated noise level is noticeable in the 4.5 Å wavelength channel. Only three most attenuative materials (Cu, Fe and Ni) are visible in sinograms; Zn and Al are obscured in higher levels of noise.

For comparison purposes, the images were reconstructed using filtered backprojection implemented as `FBP` in CIL with a Hann filter (fig. 2, bottom row). As expected, FBP produces extremely noisy reconstructions. Only Ni is clearly visible in the reconstructed cross-section. Reconstruction of 4.5 Å wavelength channel is substantially noisier due to both lower incident flux and lower neutron attenuation of the selected materials.

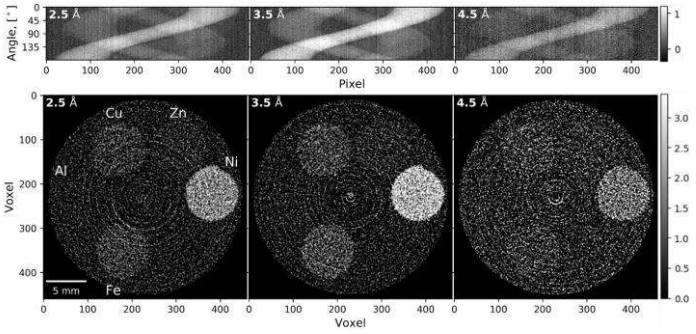

Fig 2. Top row: Sinograms for selected wavelength channels. Bottom row: FBP reconstruction of the selected sinograms.

2.2. Reconstruction

In every detector channel $k, k = 1, \dots, K$, where K is the total number of channels, the measurement model in neutron CT can be well approximated by the Beer-Lambert law. Let us consider an incident beam of neutrons of given intensity I_0 at specific wavelength λ_k, the intensity I which reach the detector element, will be reduced according to:

$$I(\lambda_k) = I_0(\lambda_k) \exp(-\int_L \mu(x, \lambda_k) \mathrm{d}x),$$

where L is a linear path through the object and μ is the wavelength-dependent attenuation coefficient at the physical position x in the object. Given an appropriate discretisation of Radon transform A (projection operator), tomographic reconstruction in every wavelength channel k can be modelled as a system of linear equations:

$$\bar{b}(\lambda_k) = -\ln\left(\frac{I(\lambda_k)}{I_0(\lambda_k)}\right) \approx \bar{A}\bar{u}(\lambda_k), \qquad (1)$$

where $\bar{b}$ is the discrete measured data, $\bar{u}$ is the to-be-reconstructed attenuation map discretised onto a Cartesian grid. The attenuation map $\bar{u}$ is typically represented as a column vector with $N = D^2$ elements (voxels), where D is the number of elements in a detector row. The discrete measured data $\bar{b}$ is vectorised as a column vector with $M = PD$ elements (pixels), with P being the total number of projections. The projection operator $\bar{A}$ contains $M \times N$ elements. If $i, i = \{0, 1, \dots M-1\}$ and $j, j = \{0, 1, \dots, N-1\}$, then $\bar{a}_{i,j}$ is the length of intersection of the i.th ray with the j.th voxel.

Similar to low-dose medical CT, the problem (1) is ill-posed in mathematical sense. Therefore, we seek for a way to compensate for the ill-posedeness of the problem by incorporating some prior knowledge about the solution. Unlike channel-by-channel methods which reconstruct each channel individually, we explore methods to jointly reconstruct all channels and exploit interchannel correlations. Then, the spectral CT data is modeled as

$$b = Au,$$

where b and u are obtained by stacking K column vectors $\bar{b}(\lambda_k)$ and $\bar{u}(\lambda_k)$, respectively, and $A = I_{K\times K} \otimes \bar{A}$, $\otimes$ is the Kronecker product, and $I_{K\times K}$ is the identity matrix of order K. The reconstruction problem is formulated as

$$\arg\min\{F(u) = f(b, Au) + \alpha g(u)\},$$

where $f(b, Au)$ is a data fidelity metric which measures the discrepancy between the projection of solution u and the acquired data b. The regularisation term $g(u)$ penalises undesired solutions and "guides" the optimization algorithm towards a solution with expected properties, which are commonly formulated in terms of image smoothness and sharp boundaries. The parameter α balances two terms and has to be tuned for each specific regulariser and dataset.

TNV is a recent extension of TV for multichannnel images [3-5]. TNV encourages the rank-sparsity by penalising the singular values of the Jacobian matrix. TNV has similar properties to TV regularisation, *i.e.* it also

promotes a sparse image gradient in the spatial dimension, but also favours reconstructions with common edges across all channels. Consequently, TNV correlates channels and improves reconstruction quality by promoting common structures in multichannel images. The reconstruction problem is then formulated as,

$$F(u) = \|Au - b\|_2^2 + \alpha \mathrm{TNV}(u). \quad (2)$$

Similar to TV, TNV suffers from a loss of contrast. Secondly, TNV does not allow the decoupling of regularisation parameters for the spatial and spectral dimensions which makes impossible to balance the level of regularisation between dimensions.

Here, we propose a novel tailored regulariser which combines TV [6,7] in the spatial dimension with TGV [8] the spectral (channel) dimension to jointly reconstruct low-count multi-channel neutron CT data. The proposed approach allows enforcing different image properties in respective dimensions. As the TV model captures piece-wise constant image properties in the spatial dimension, we rely on another regulariser to support reconstruction in the spectral dimension. Here, we rely on TGV to recover piece-wise smooth features in the spectral dimension because TGV allows balancing the first and the higher-order derivatives of images and consequently alleviates the staircasing effect inherent to TV. In this case the reconstruction problem is formulated as,

$$F(u) = \|Au - b\|_2^2 + \beta \mathrm{TV}_{x,y,z}(u) + \gamma \mathrm{TGV}_c(u). \quad (3)$$

Here we use $\mathrm{TV}_{x,y,z}$ to designate a TV operator over three spatial dimensions x, y and z, whereas TGV_c operates over the spectral (channel) dimension.

Both methods (2) and (3) were implemented based on the CCPi Core Imaging Library (CIL) [9, 10]. CIL wraps the ASTRA toolbox [15] to perform forward- and back-projection operations and provides a set of various regularisers through the CCPi Regularisation Toolkit [16]. FISTA [17] and PDHG [18] were used to solve (2) and (3), respectively. Regularisation parameters were chosen manually to achieve both noise suppression and feature preservation in both spatial and spectral dimensions (α=0.01, β=0.0075 and γ=0.3).

3 Results

Fig. 3 shows two-dimensional slices for selected (individual) wavelength channels reconstructed using the regularised iterative methods discussed in this paper. Both TNV and TV+TGV demonstrate drastic improvement in reconstruction quality and noise suppression. TNV produces "patchy" images and smearing of features is visible especially between the Cu and Zn cylinders (fig. 3, top row). Overall, features appear sharper in the TV+TGV reconstruction (fig. 3, bottom row).

TNV uses a small pixel neighbourhood information to correlate structural information along the spectral dimension. This acts similarly to a low-pass filter. Thus, TNV suppresses ring artifacts visible in FBP reconstruction (fig. 2) but causes blurred and enlarged rings especially prominent in 4.5 Å channel, where counts are much lower. Al has very low neutron attenuation and is invisible in the TNV reconstruction due to contrast loss; a known drawback of both TV and TNV regularisation methods.

The TV+TGV reconstruction does not suffer from the ring artefacts and the faint Al cylinder is distinguishable in the reconstructed slices and profile lines (fig. 4, bottom row). Fine features inside the Cu cylinder are also partially preserved in the TV+TGV reconstruction (fig. 4, top row).

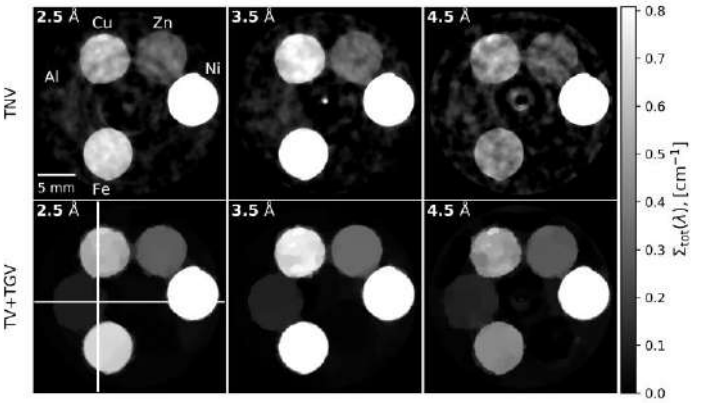

Figure 3: Two dimensional reconstructions of selected (individual) wavelength channels reconstructed with TNV regularisation (top row) and with TV+TGV regularisation (bottom row). White lines mark profile lines chosen for examination in the next figure. All slices are visualised with a common colour range. Colour range was adjusted to highlight low intensity features (maximum value of the display range was set to 30% of maximum intensity value in the reconstructed volume).

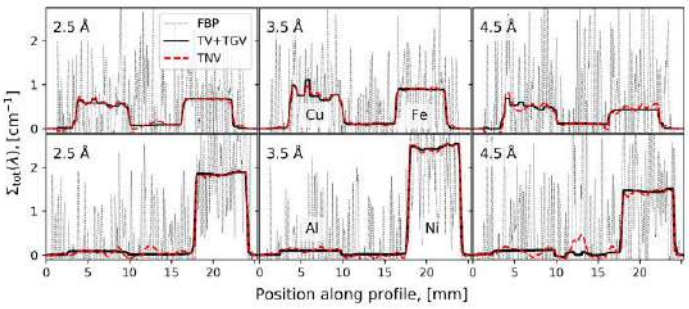

Figure 4: Profiles corresponding to the vertical (top row) and horizontal (bottom row) white lines in figure 3 (bottom left) passing through the Cu and Fe cylinders and the Al and Ni cylinders, respectively.

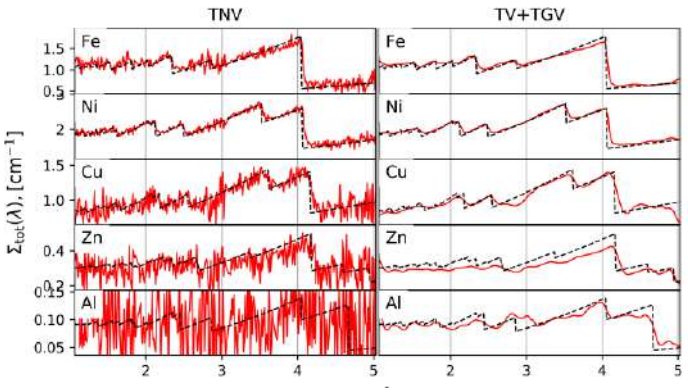

Figure 5: Individual spectra (solid line) reconstructed with TNV and TV+TGV for one representative 0.055^3 mm^3 voxel located within each material alongside the theoretical predictions (dotted black line).

Individual spectra reconstructed for one 0.055^3 mm^3 voxel in each of the 5 materials are plotted in fig. 5 alongside the theoretical predictions. The voxel locations inside the cylinders were chosen arbitrarily. The reconstructed spectra for Fe, Ni and Cu closely follow the predicted spectra for both TNV and TV+TGV reconstructions. The amplified noise visible in the TNV reconstructions between 2.5 Å and 3 Å is caused by the increased noise levels in input data due to the detector dead time [14]. While the TV+TGV produces a much smoother spectra the Bragg edges appear to be less prominent due to smearing (for instance, small edges around 2 Å in Fe). In the case of the TNV regularisation, the noise dominates over smaller Bragg edges. For the materials with lower neutron attenuation (Al and Zn), TV+TGV clearly outperforms TNV as some Bragg edges are visible in the reconstructed spectrum, but are completely lost in the noise in the case of TNV.

Reconstruction is an intermediate step in Bragg edge imaging. The Bragg edge positions (in terms of *d*-spacing) allows compositional mapping, as each crystalline structure has a unique set of lattice spacings and hence a fingerprint in the neutron transmitted spectrum. The shape of the detected Bragg edges, *i.e.* deviation from abrupt predicted edge, supports characterisation of crystallographic properties. Quantitative comparison of the reconstruction results in terms of Bragg edge detection and characterisation, as well as material decomposition is a topic of future work.

5 Conclusion

We have demonstrated the capabilities of advanced reconstruction methods to improve reconstruction quality of low-count ToF neutron CT data. We investigated application of two regularisation techniques: the dedicated regulariser for multi-channel CT data and the tailored regularisation term encoding the prior information about neutron spectra. Both regularisation techniques showed drastic improvement of reconstruction quality compared to the standard FBP method. The tailored regularisation provided better reconstruction quality. Our study serves as an initial demonstration of a dedicated reconstruction technique that facilitates significant reduction of required exposure time – a major bottleneck in low flux ToF neutron CT studies.

5 Funding

This work was funded by EPSRC grants “A Reconstruction Toolkit for Multichannel CT” (EP/P02226X/1), “CCPi: Collaborative Computational Project in Tomographic Imaging” (EP/M022498/1 and EP/T026677/1). We gratefully acknowledge beamtime RB1820541 at the IMAT Beamline of the ISIS Neutron and Muon Source, Harwell, UK. EA was partially funded by BMBF and the Baden-Württemberg Ministry of Science as part of the Excellence Strategy of the German Federal and State Governments. JSJ was partially supported by The Villum Foundation (grant No. 25893). WRBL acknowledges support from a Royal Society Wolfson Research Merit Award. PJW acknowledges support from the European Research Council grant No. 695638 CORREL-CT.

References

[1] K. Watanabe et al. “Cross-sectional imaging of quenched region in a steel rod using energy-resolved neutron tomography.” Nuclear Instruments and Methods in Physics Research Section A 944 (2019): 162532. DOI: 10.1016/j.nima.2019.162532

[2] C. Carminati et al. “Bragg-edge attenuation spectra at voxel level from 4D wavelength-resolved neutron tomography.” Journal of Applied Crystallography 53.1 (2020): 188-196. DOI: 10.1107/S1600576720000151

[3] K. M. Holt “Total nuclear variation and jacobian extensions of total variation for vector fields.” IEEE Transactions on Image Processing 23.9 (2014): 3975-3989. DOI: 10.1109/TIP.2014.2332397

[4] D. S. Rigie and P. J. La Rivière. “Joint reconstruction of multi-channel, spectral CT data via constrained total nuclear variation minimization.” Physics in Medicine & Biology 60.5 (2015): 1741. DOI: 10.1088/0031-9155/60/5/1741

[5] D. Kazantsev et al. “Joint image reconstruction method with correlative multi-channel prior for x-ray spectral computed tomography.” Inverse Problems 34.6 (2018): 064001. DOI: 10.1088/1361-6420/aaba86

[6] L. I. Rudin, S. Osher, and E. Fatemi. “Nonlinear total variation based noise removal algorithms.” Physica D: nonlinear phenomena 60.1-4 (1992): 259-268. DOI: 10.1016/0167-2789(92)90242-F

[7] E. Y. Sidky, C.-M. Kao, and X. Pan. “Accurate image reconstruction from few-views and limited-angle data in divergent-beam CT.” Journal of X-ray Science and Technology 14.2 (2006): 119-139.

[8] K. Bredies, K. Kunisch, and T. Pock. “Total generalized variation.” SIAM Journal on Imaging Sciences 3.3 (2010): 492-526. DOI: 10.1137/090769521

[9] J. Jørgensen et al. “Core Imaging Library – Part I: a versatile Python framework for tomographic imaging”. Philosophical Transactions of the Royal Society A (submitted) (2021).

[10] E. Papoutsellis et al. “Core Imaging Library – Part II: Multichannel reconstruction for dynamic and spectral tomography”. Philosophical Transactions of the Royal Society A (submitted) (2021).

[11] W. Kockelmann et al. “Time-of-flight neutron imaging on IMAT@ ISIS: a new user facility for materials science.” Journal of Imaging 4.3 (2018): 47. DOI: 10.3390/jimaging4030047

[12] G. Burca et al. “Modelling of an imaging beamline at the ISIS pulsed neutron source.” Journal of Instrumentation 8.10 (2013): P10001.
DOI: 10.1088/1748-0221/8/10/P10001

[13] A. S. Tremsin et al. “High resolution photon counting with MCP-Timepix quad parallel readout operating at > 1 KHz frame rates.” IEEE transactions on nuclear science 60.2 (2012): 578-585. DOI: 10.1109/TNS.2012.2223714

[14] A. S. Tremsin et al. “Optimization of Timepix count rate capabilities for the applications with a periodic input signal.” Journal of Instrumentation 9.05 (2014): C05026. DOI: 10.1088/1748-0221/9/05/C05026

[15] W. Van Aarle et al. ‘Fast and flexible X-ray tomography using the ASTRA toolbox.” Optics express 24.22 (2016): 25129-25147. DOI: 10.1364/OE.24.025129

[16] D. Kazantsev et al. “CCPi-regularisation toolkit for computed tomographic image reconstruction with proximal splitting algorithms.” SoftwareX 9 (2019): 317-323. DOI: 10.1016/j.softx.2019.04.003

[17] A. Beck and M. Teboulle. “A fast iterative shrinkage-thresholding algorithm for linear inverse problems.” SIAM journal on imaging sciences 2.1 (2009): 183-202. DOI: 10.1137/080716542

[18] A. Chambolle and T. Pock. “A first-order primal-dual algorithm for convex problems with applications to imaging.” Journal of mathematical imaging and vision 40.1 (2011): 120-145. DOI: 10.1007/s10851-010-0251-1